Humidity-Resistant, Broad-Range Pressure Sensors for Garment-Integrated Health, Motion, and Grip Strength Monitoring in Natural Environments

S. Zohreh Homayounfar, Ali Kiaghadi, Deepak Ganesan, and Trisha L. Andrew*

Wearable electromechanical sensors are essential to improve health monitoring and off-site point-of-care applications. However, their practicality is restricted by narrow ranges of detection, failure to simultaneously sense static and dynamic pressures, and low durability. Here, an all-fabric pressure sensor with high sensitivity in a broad range of pressures, from subtle heart pulses to body posture, exceeding that of previously-reported sensors is introduced. By taking advantage of chemical vapor deposition of p-doped poly(3,4-ethylenedioxythiophene) chloride (PEDOT-Cl) on two natural textiles (cotton gauze and cotton balls), multiscale tunable pressure sensitivity with low power demand for data read-out is obtained. To protect the sensor against humidity induced degradations, the sensor is encapsulated with a hydrophobic coating that leads to ultrastability of the sensor performance even after 1 week of exposure to 100% relative humidity and 20 laundry cycles. The sensor reveals excellent performance retention of >99% over 70 000 bending cycles under ambient conditions. The varied utility of this sensor for health monitoring is demonstrated by recording heartbeats, respiration, and joint movements. Furthermore, using this sensor, grip strength is successfully detected by 93.6% accuracy as compared to commercial dynamometer, speaking of its potential as the first fabric-based sensor allowing for personalized real-time grip strength analysis.

S. Z. Homayounfar, T. L. Andrew
Department of Chemistry
University of Massachusetts of Amherst
Amherst, MA 01003, USA
E-mail: tandrew@umass.edu
A. Kiaghadi
Department of Electrical Engineering
University of Massachusetts of Amherst
Amherst, MA 01003, USA
A. Kiaghadi, D. Ganesan
College of Information and Computer Science
University of Massachusetts of Amherst
Amherst, MA 01003, USA
T. L. Andrew
Department of Chemical Engineering
University of Massachusetts of Amherst
Amherst, MA 01003, USA

1. Introduction

The advancement of wearable electromechanical pressure sensors for detecting biopotentials and body locomotion is critically essential in evaluating human performance and improving personalized point-of-care applications.[1–4] In the paradigm of off-site health monitoring, one of the key features of pressure sensors which is still unmet is their ability to sense subtle (1 Pa–10 kPa) dynamic pressures such as heart beats while being already under the application of a medium (10–100 kPa) or large (>100 kPa) static pressure such as the pressure applied by the body as the person is lying in the bed.[5–7] Moreover, some aspects of the health monitoring applications such as grip strength measurement have not yet been taken care of among the wearables community.[8,9] Grip strength is a crucial health indicator closely interrelated to aging, degree of training and rehabilitation, and/or special muscular diseases in children under 5 years old.[10,11] Measuring grip strength has been highly limited by the commercial dynamometers which mostly fail to be used for long-term monitoring of grip strength specially in more sensitive target population such as babies or rehabilitation patients.[8,9,12] Thus, there is a dire need for a comfortable, yet sensitive wearable sensor which enables real-time grip strength detection in daily life.

Piezoresistive pressure sensors, in which the ultimate electrical output is resistance variations, are the most-widely used class of electromechanical sensors due to the simplicity of read-out system in signal acquisition, simple working mechanism that allows a wide variety of materials to be used along with cost-effective fabrication processes.[5,13] A key challenge in developing these sensors is having an acceptably high sensitivity in a broad range of detection (RoD), defined as the range between the lowest and the highest amount of pressure being distinguishable by the sensor.[14] Skin-contact piezoresistive pressure sensors, that are considered the most frequently reported one, basically have an elastomeric backbone filled with conductive nano- or microstructures, allowing for percolation mechanism to get into action.[15–18] These sensors have RoD in the range of subtle to medium pressures and are highly restricted by

**ADVANCED
SCIENCE NEWS**
www.advancedsciencenews.com

**ADVANCED
MATERIALS
TECHNOLOGIES**
www.advmattechnol.de

the mechanical properties of the elastomer along with lack of breathability.[19,20]

Conceptually, replacing elastomers with textiles sounds like a descent solution to overcome difficulties posed on the functionality and sensitivity of the piezoresistive sensors. Textile-based piezoresistive pressure sensors could expand the RoD in pressure sensitivity by leveraging two main structures. One structure belongs to the point-to-point connection-disconnection sensors in which a porous, insulate 3D spacer is placed between two conductive fabrics and creates an architectured piezoresistive structure.[21,22] Since these sensors perform in between on/off switching states and also, due their relatively low durability resulted from the gradual dysfunctionality of the middle spacer, their true practicality is narrowed down to tactile feedback applications.[22] The second structure which is the basics for the majority of so far developed textile-based piezoresistive pressure sensors is the typical sandwich structure including two electrodes holding a conductive active layer in between. Different approaches have been adopted to render the textiles conductive such as coating fibers with conductive inks[23] and polymers,[24,25] or developing conductive yarns using one or combination of conductive nanoparticles[26–29] and intrinsically conductive polymers (ICPs)[25] or MXenes,[30,31] followed by weaving or attaching to patterned electrodes for point-to-point connection. Although these techniques have led to extended RoD window in some cases, they still suffer from major drawbacks such as either saturation or high electromagnetic noise due to highly conductive coatings, degradation resulted from exposing to sweat and aging in daily applications, and most importantly failure to sense multiple dynamic/static pressures at the same time. In fact, those who deal with monitoring physiological signals and human activity monitoring through wearable electronics know that having access to multimodal sensing capabilities is not any less essential than enjoying a high sensitivity in a broad range of pressures.

Recently, we introduced a piezoionic pressure sensor, called "PressION,"[32,33] which was capable of sensing signals simultaneously in both static and dynamic contexts with a wide range of detection. The active layer of this sensor was made of regular cotton gauze fabric coated with a quaternary ammonium siloxane through solution processing. The aim of the current study is to extend the quality of that structure to a higher level of practicality and wide-adoptability by taking advantage of chemical vapor deposition (CVD). CVD enabled us to coat unconventional textures and allows for taking advantage of the fuzziness of natural 3D structures in a one-step, solution-free process to be used as an active layer in the sensor. Our new sensor enjoys three active working mechanisms in three different length scales: reduction of the active layer thickness in milli-centimeter scale, percolation due to hierarchical arrangement of the coated/uncoated fibers and the continuity breaks in the polymeric coatings in milli-micrometer scale, and the piezoionic effect or redistribution of ions in nanometer scale. The simultaneous activity of all these mechanisms led to the ability of the sensor to detect subtle dynamic pressures while being under the application of a large static base pressure. Furthermore, while we leveraged the presence of ions in the active layer, we addressed all the drawbacks entangled with their high sensitivity to humidity by encapsulating the sensor through vapor deposition of hydrophobic moieties.[34] The hydrophobicity nature of this sensor leads to its high stability against sweat and laundry cycles, making it outstand among other reported wearable pressure sensors. This sensor is considered a passive sensor as it exhibits variations in resistance as a result of change in applied pressure that can be read with the slightest amount of operating voltage. We explored the sensitivity and performance of the sensors in a wide-range of static and dynamic pressures and a variety of real-time physiological and human motion signal detection. Finally, we evaluated the sensor performance in grip strength measurement as compared to household dynamometer, speaking of its potential as a first-of-its kind fabric-based grip strength detector.

2. Results and Discussion

2.1. Fabrication of the Poly(3,4-ethylenedioxythiophene) Chloride (PEDOT-Cl) Vapor Printed Pressure Sensor

In designing a piezoresistive sensors, the common strategy is to have a two conductive layer as the electrodes and one reasonably resistive active layer sandwiched in between. However, the key challenging point in reaching high sensitivity and broad range of detection is to tune the resistance of the active layer accordingly. If the active layer is too resistive (teraOhms), such as pristine cotton, the sensor will play as a great electromagnetic receptor which will greatly reduce signal to noise ratio. On the other hand, a very conductive sensor will have lower sensitivity to pressure while requiring more power to be read. Thus, there is a sweet spot region of resistivity allowing for optimal performance of the sensor, where it does not induce electromagnetic noises and does not negatively affect the sensor sensitivity.

To address this issue, we developed two types of active layers with tunable resistivity by leveraging chemical vapor deposition of *p*-doped PEDOT-Cl. In the CVD process, polymer coatings are grown directly on a target surface by simultaneously introducing monomer and oxidant vapors into a custom-built hot-wall reaction chamber (**Figure 1**A) equipped with a substrate stage, controlled inlet for monomer vapor delivery and a heated crucible to vaporize the oxidant. The monomer and the oxidant vapors meet at the heated stage placed over the crucible and initiate the polymerization reaction on any exposed face of any substrate sitting in that region (Figure 1B). Mechanistically, simultaneous introduction of monomer and oxidant vapors into the reaction chamber allows radical cations of the monomer to form in high concentration, in the vapor phase, prior to dimerization (Figure 1B). Because dimerized species have significantly lower vapor pressures relative to their corresponding monomers, polymer growth, and chain extension likely occurs on the substrate surface. The presence of excess metal salts throughout the deposition further oxidizes the polymer film, leaving behind *p*-doped PEDOT-Cl. Subsequent rinsing of the as-deposited films with water removes metal salts, excess oxidant, and any soluble byproducts trapped within the film. The overall thickness of the PEDOT-Cl coating is controllable by adjusting the monomer flow rate as well as the duration of the vapor deposition process, which gives us the opportunity to tune the resistivity of the active layer. Second,
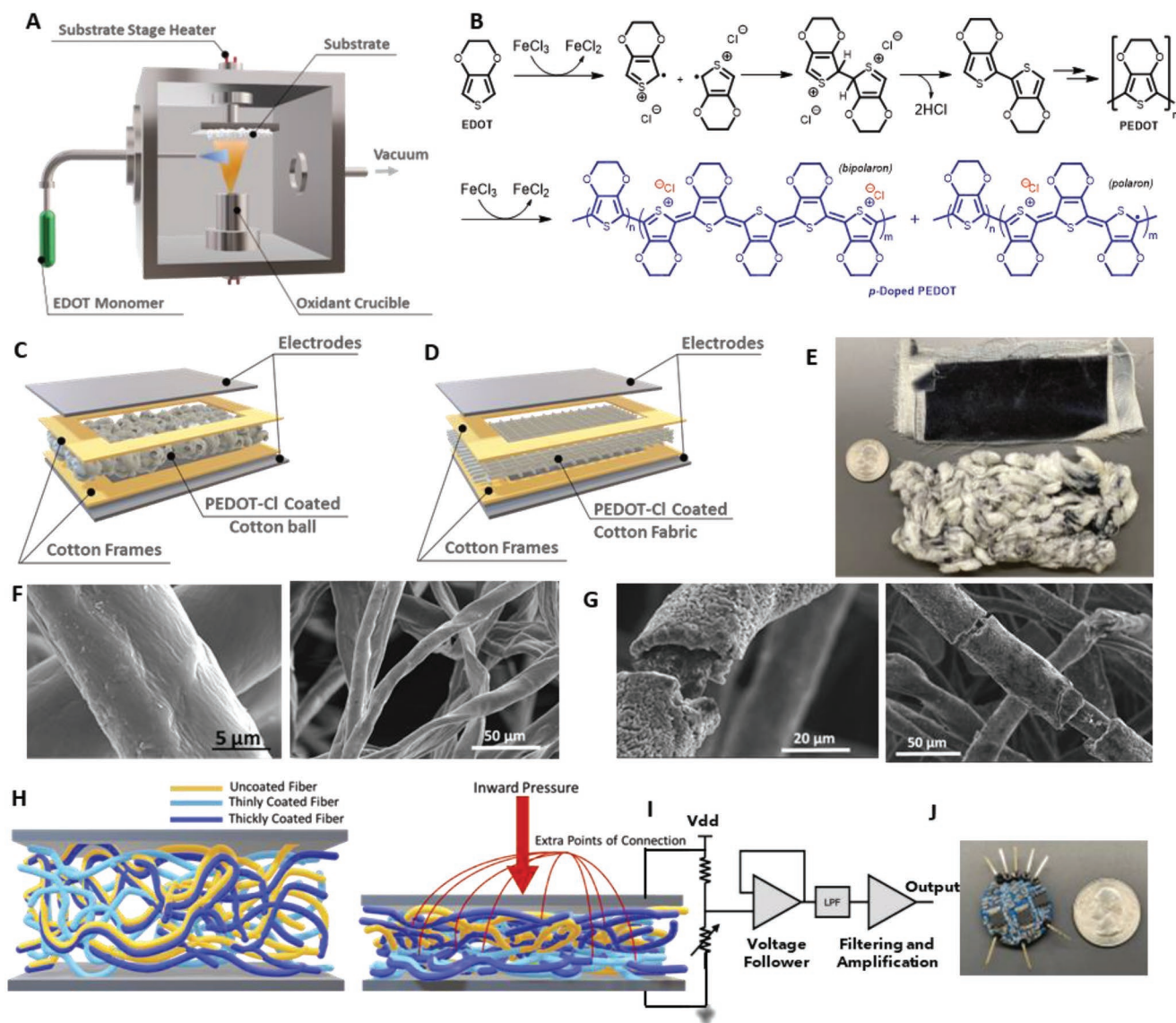
ADVANCED
SCIENCE NEWS

www.advancedsciencenews.com

ADVANCED
MATERIALS
TECHNOLOGIES

www.advmattechnol.de

Figure 1. Fabrication process and Working Mechanism of the Sensor: A) Schematic illustration of the custom-built Chamber used for oxidative chemical vapor deposition (oCVD). B) Polymerization reaction and chemical structure of p-doped PEDOT-Cl created by CVD. C,D) Schematic illustration of sensor structure with C) cotton ball, D) cotton fabric as the active layer. E) Photograph of PEDOT-Cl coated fabric cotton versus fluffed structure of PEDOT-Cl coated cotton ball. F) Scanning electron microscopy image of cotton ball single fiber (on the left) and bunch of fibers (on the right). G) Intentional discontinuity breaks in the PEDOT-Cl coating of cotton ball leading to more percolation pathways. H) Schematic illustration of pressure sensor with a combination of uncoated, thinly coated, and thickly coated fibers which under the application of an inward pressure reaches to higher number of point of connectivity and therefore lower resistivity. I,J) The equivalent circuit model of the sensor controller board I) and its photograph J).

this technique enables us to coat not only fabrics with different textile parameters, such as weave density, but also to coat unconventional but still comfortable-to-wear textures such as cotton ball. Thus, in this design we have the option to change the type, thickness, number of layers of the fabric as well as changing the thickness of the coating and therefore, tune and adjust the sensitivity of the sensor depending on the requirements of the corresponding application. These options were not viable with our previously reported pressure sensor (PressION) developed through solution processing.

We vapor printed PEDOT-Cl on two different textures: cotton fabric and cotton balls. Our first sensor was made with

PEDOT-Cl coated cotton fabric as an active layer (Figure 1D). After exploring the impact of wave density and thickness of different fabrics on the overall resistivity of the sensor, we found that the thin, loose-weave cotton voile gave us the best pressure-indued signal quality. Usually by vapor deposition on thick and tight/medium-weave fabrics, only one face of the target fabric swatch can be selectively coated. However, the thin thickness and loose-weave mesh of the selected cotton voile, let the polymer traces leak into the other face of the swatch, making the transduction mechanism required for sensing quite possible. As seen in Figure S1 (Supporting Information), the difference in the weave density of the normal cotton and the cotton

voile used in this study is quite distinguishable. This feature enabled us to further tune the resistivity as well as sensitivity of the sensor by adding/removing the number of layers between the electrodes. The optimized PEDOT-Cl coated active layer was then sandwiched between two silver nylon fabric swatches playing the role of electrodes in the system. In order to minimize shorting events, we used regular cotton fabric as a frame to hold the active layer in between and prevent the electrodes from getting in contact with each other (Figure 1D).

In order to reach to a wider range of signal detection we needed to explore a more widely spaced disordered structure that can be firmly pressed under the application of any amount of pressure. Cotton balls enjoyed this structure, in addition to the fact that, as opposed to synthetic structures, we still could benefit from the chemically reactive hydroxyl groups available on the cellulose surface serving as principal sorption sites for substitution reactions and crosslinking. Thus, our second sensor was made with PEDOT-Cl coated cotton ball (Figure 1C). To the best of our knowledge, this was the first time that cotton ball was successfully used as a substrate for a conjugated polymer vapor deposition. Due to the densely crowded and entangled structure of the cotton ball, the polymeric film covers only the face exposed to the polymerization region. Thus, we later fluffed up the coated cotton ball to get a uniform dispersion of coated fibers among the uncoated ones (Figure 1E). By introducing more coated fibers into the fluffy layer, we can tune the resistivity of the layer. Obviously, the more we fill the layer with the coated fibers, the lower the overall resistivity of the sensor becomes. The thickness of the fluffy layer is also another option to tune the resistivity along with sensitivity of the sensor. This fluffed-up coated cotton ball layer was then placed between the cotton frame and the silver nylon electrodes as shown in Figure 1D.

While taking advantage of the presence of ions in our sensor, we protected the sensor against all the humidity-induced degradations entangled with ions and other aging processes such as laundry cycling via vapor deposition of hydrophobic moieties over all the sensor layers. By using another custom-built vacuum reactor, we successfully coated trichloro (1H,1H,2H,2H-perfluorooctyl)silane (TCPFS) all over the sensor layers before assembling them together. As shown in Figure S2 (Supporting Information), this coating provides the fabrics surfaces with high hydrophobicity and thus, prevent the water molecules from penetrating into the structure and degrade the PEDOT-Cl conductivity. We measure water contact angle with the fabric surface through goniometer for 5 times. The mean was 134.88° with the standard deviation of 0.132°, which is indicative of high hydrophobicity of the surface (Figure S2C, Supporting Information).

The scanning electron microscopy (SEM) images of a single uncoated cotton ball fiber reveals the striations of individual fibers (Figure 1F). After being coated with PEDOT-Cl, the striations are no longer observed, and the deposited polymer film wraps around the circumference of the fiber uniformly in case of cotton fabric (Figure S3, Supporting Information) and non-uniformly in case of cotton ball (Figure 1G). This observation speaks again to the effectiveness of vapor deposition technique for coating conjugated polymers on topographically complex and unconventional substrates, such as cotton ball. In Section

2.2., we will talk more about how we take advantage of this intentional continuity breaks in cotton ball coating.

2.2. Principles of Working Mechanism

Regarding the principles of working mechanism of the sensor, we believe there are three active phenomena simultaneously taking place in the sensor in different length scales. First, as shown in Figure 1H upon the application of an inward pressure, we have the reduction of the thickness of the active layer and therefore, the putative decrease in the air trapped between the fibers in milli-centimeter scale, both of which lead to the overall decrease in the sensor resistivity according to the well-known equation of resistance

$$R = \rho \frac{l}{A} \tag{1}$$

where ρ is the electrical resistivity, l is the length, and A is the cross-sectional area of the medium. By getting rid of the air, we have a reduction in ρ, as the air is insulate, and in l as we decrease the length of the medium.

Second, the intentional hierarchical arrangement of coated/uncoated fibers in the active layer along with the continuity breaks in the polymeric coating, shown in the SEM images of the active layer in Figure 1G, that is automatically produced by the vapor deposition method followed by fluffing out the cotton balls, allows for percolation pathways/thresholds to come into effect and extends the sensing window to milli-micrometer scale. When we press the sensor, we provide the charge carriers with more points of connectivity (Figure 1H) and thus, get lower resistivity. Thus the disorder nature of the fabric weave and the "fuzziness" of the cotton ball add to the effectiveness of this mechanism.

Third and last, PEDOT-Cl, as a doped conducting polymer, has a combination of ions and electrons as its charge carriers. Energy-dispersive X-ray spectroscopy (EDX) of the active layer confirmed the persistence of chlorine atoms (Figure S4, Supporting Information). Thus, in addition to the transduction mechanism observed in normal electron-based conductive active layers, we take advantage of the presence of chloride counter ions in the system. These ions provide the sensor with piezoionic effect in which the application of a compression stress results in the redistribution of ions in the system in nanoscale, leading to a subtle change in the resistance. Therefore, even if the sensor is squished by a large pressure such as body weight, still the percolation part and the piezoionic part allow for small added pressures, such as heartbeats, to be detected. This ability of the sensor to detect both dynamic and static added pressures while being already under the application of a base static pressure will be thoroughly explored in Sections 2.3.

In order to further explore the activity of the counter ions in this structure, we studied the temperature variation of electrical resistivity of the sensor in the liquid nitrogen temperature range. Figure S5 (Supporting Information) reveals that the electrical resistivity of the sensor increases with the decrease in the temperature. Moreover, an almost linear relationship is

**ADVANCED
SCIENCE NEWS**

www.advancedsciencenews.com

**ADVANCED
MATERIALS
TECHNOLOGIES**

www.advmattechnol.de

observed between the electrical resistivity and $T^{-1/4}$, the typical relationship known for other conjugated polymer composites.[35] Thus, it can be deduced that we have a composite structure made of an insulating polymer phase (Cotton fibers) and a conductive polymer phase (PEDOT-Cl) where the conducting network are principally based on the direct inter-particle contacts. This observation further confirms the presence of percolation working mechanism discussed before.

2.3. System Design for Data Acquisition

As already mentioned, the sensor performs by translating the changes in the applied pressure into the changes in its resistance. In order to capture these changes, when we are dealing with DC signals, it is more straightforward to record the change in the sensor resistance. However, once we are dealing with the fast dynamic responses like capturing physiological signals, recording voltage has preference over resistance. Thus, to facilitate the process of data acquisition and clear the way for the future applications of the sensor in daily life, we designed a button-sized PCB board (Figure 1J), in which we deploy a voltage divider circuit where a constant resistor is placed in series with the sensor and the output voltage is measured in the common node (Figure 1I). To isolate the loading effect stemmed from Analog to Digital Converter (ADC), we use a unity gain amplifier as a voltage buffer.

During the experiments where base pressure is changed, and to negate the effect of electronics in our performance evaluations, we modify the constant resistor to keep the base line at the same level. This is due to the fact that as output voltage reaches toward *GND* or *VCC*, the board saturates in terms of voltage and limits the sensor response. Moreover, to find minute pressure changes, such as heartbeat pulses, this signal needs to be amplified, and the DC portion as well as high frequency noise need to be rejected. Thus, a second order active filter is used to amplify and filter the signal.

2.4. Comparing Sensors Performance in Static and Dynamic Contexts

As discussed before, one of the most important challenges that has limited the practicality of the so-far developed pressure sensors is their failure to detect subtle dynamic/static pressures such as heartbeat while being under the application of an initial static pressure such as body weight. We simulated this condition by designing an experiment (**Figure 2**A) in which in order to approximate a static base pressure we placed a 1 and then 2 kg copper plate on top of the sensor in sequence, and then applied an extra inward compression stress as the extra static pressure. As seen in Figure 2B,C, both sensors remained highly sensitive even in the presence of a constant base pressure of 2 kg, which is close to the average pressure exerted by the body weight while sleeping on a bed. The sensor with cottonball shows a slightly deeper drop with initial weight which is due to the damping effect of its fuzzy structure. Another important feature revealed in this experiment is the reversibility of the base resistance of the sensor which obviously leads to repeat-

ability of the measurements. As shown in Figure 2B,C, both sensors show full return to their initial base line after removing the pressures, which is a promising performance, specifically for the sensor filled with cotton ball with its fuzzy nature.

We compared the sensitivity and the range of variations in our two sensors by placing a range of weights with the same surface area on the sensors to approximate the exertion of a wide range of pressures. We repeated this measurement 10 times for each weight and the results were box plotted in Figure 2E. Both sensors showed the same trend of decrease in the resistance upon the increase in the applied pressure. As seen in figure 2D, they revealed extremely high level of sensitivity for subtle to small pressures with lower but still quite acceptable range of sensitivity for ultra-high pressures (almost 50 times larger than human body pressure on the bed). The sensor filled with cotton ball as the active layer exhibited slightly lower range of variation and lower error for the same amount of sensitivity. This lower range of variation and higher precision can be attributed to the higher number of points of connectivity available due to its fuzziness providing the charge carriers with more percolation pathways.

Next, in order to evaluate the dynamic sensitivity of the sensors under the application of a static base pressure, we reperformed the same experiment with 1 and 2 kg copper plates on top of the sensor to approximate the static base pressure, but this time we simulated the extra dynamic pressure by dropping a bouncing ball on the sensor from a specific height (Figure 2F). As shown in Figure 2G, the static pressure leads to a drop in the base line of the signal and then each impact of the bouncing ball on the sensor turns into a sudden deep drop in the voltage signal. The average magnitude of all those peaks for each experiment was plotted in Figure 2H. Both sensors were extremely responsive to dynamic pressures with or without the presence of static base pressure. In the absence of base pressure, the sensor filled with cotton ball shows slightly lower signal which is due the energy damping caused by the fluffy structure of the cotton ball. However, upon the application of a base pressure, its signal got even more stronger since the sensor got rid of the initial damping effect and gained access to more connectivity pathways.

2.5. Effect of Humidity on the Sensor Performance

The sensitivity of PEDOT-Cl coated fabrics to humidity is a well-known phenomenon and researchers have took advantage of this effect to develop humidity-sensitive devices.[36] However, for the current application of pressure sensing, we needed to mitigate this correlation to be able to acquire a stable and repeatable measurement in any environment regardless of the amount of humidity the sensor is being exposed to. Thus, we encapsulated the sensor with a polymeric shielding layer (TCPFS).

In order to explore the effect of humidity on the sensor performance before and after the application of the protective layer, first we studied the change in the resistance of the sensor over time in a home-built humidity chamber shown in **Figure 3**A. In this experiment, the sensor is placed in a sealed chamber, where the humidity gradually increases as the water vaporizes from a

ADVANCED
SCIENCE NEWS _____
www.advancedsciencenews.com

ADVANCED
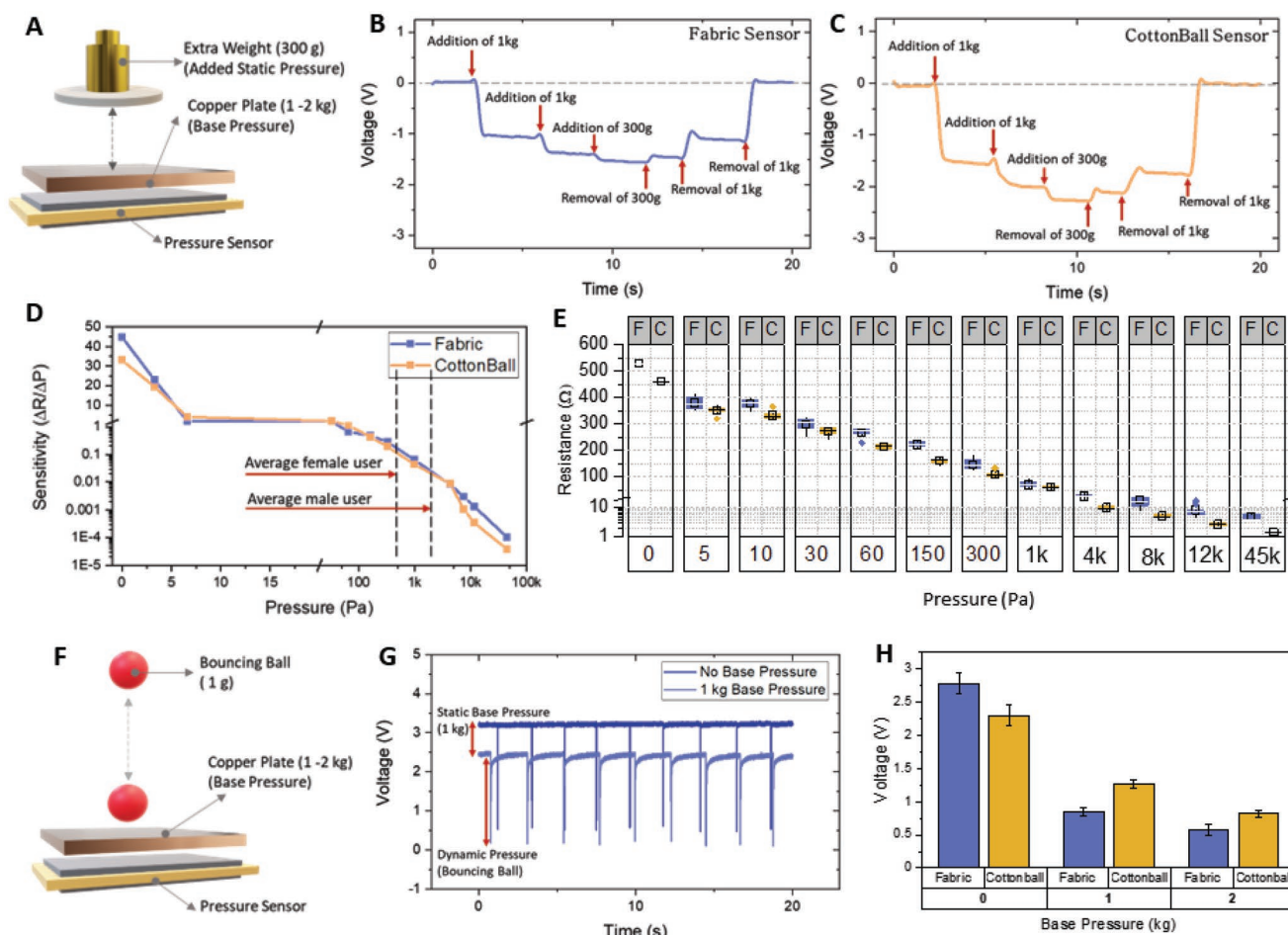MATERIALS
TECHNOLOGIES
www.advmattechnol.de

Figure 2. Comparing the performance of the pressure sensor made with fabric versus cotton ball in static and dynamic Contexts: A) Experimental setup to observe the effect of a base pressure on the static response and reversibility of the sensor. B,C) Representative real-time signal output from the sensor for the experimental setup depicted in part A) for the Fabric, B) and cottonBall sensors C), respectively, D) comparison of the sensitivity of the fabric versus cottonball sensors under the application of a wide range of static pressures. E) Boxplot illustration of the comparison of the sensor performance with Fabric versus cottonball under a wide range of pressures. F) Experimental setup to observe the effect of a base pressure on the dynamic response of the sensors. G) Representative real-time signal output from the sensor for experimental setup depicted in part. F,H) Bar plot illustration of the comparison of the sensor dynamic response with fabric versus cottonball under static base pressures.

water-soaked sponge inside the setup. The increase in the relative humidity (RH%) of the chamber was constantly monitored using a commercial hygrometer, and simultaneously the change in the resistivity of the sensor was recorded using a digital multimeter. Figure S6 (Supporting Information) shows the change in the resistance of the sensors before the encapsulation. Both the sensors with cotton and cotton ball revealed the same pattern of change in the resistance, where in the first 15 min that the humidity rose from 30% to almost 60%, we observed an increase of ≈ 9200 and $\approx 600\ \Omega$ in the sensors, respectively, and then both of their resistance gradually decreased almost 7 times after being in nearly 100% RH for a day. This pattern represents a typical behavior in PEDOT-Cl-coated natural textiles based on cellulose acetate and has been reported before. In fact, by the exposure of the sensor to humidity, the fibers tend to swell and repel each other so that they shrink away from the water. This leads to some breakage in the connectivity points between the PEDOT-Cl-coated surfaces and disappearance of fiber-fiber con-

nections in the macro level. Therefore, the nominal percolation pathways are broken which raises the resistance. By constant increase in the humidity, the water concentration becomes so overwhelming that starts to hydrate PEDOT-Cl coating itself, and the PEDOT-Cl coating becomes more conductive as it gets wet. This effect overrides that initial decline in conductivity due to the mechanical untangling of fibers and that is where the resistance keeps dropping.

When repeating the experiment with the sensors encapsulated with the protective layer, as seen in Figure 3B, we observed the same amount of initial increase in the resistance ($\approx 900\ \Omega$) but with a slower pace which shows the same trend of mechanical untangling of fibers that took place more slowly as the water had hard time penetrating between the fibers due to the overall hydrophobicity of the electrodes and the framing fabrics. Notably, after this initial increase, the resistance stayed constant with further increase in the humidity and over more than 1 week. This speaks of the fact that hydrophobicity of the encapsulating layer
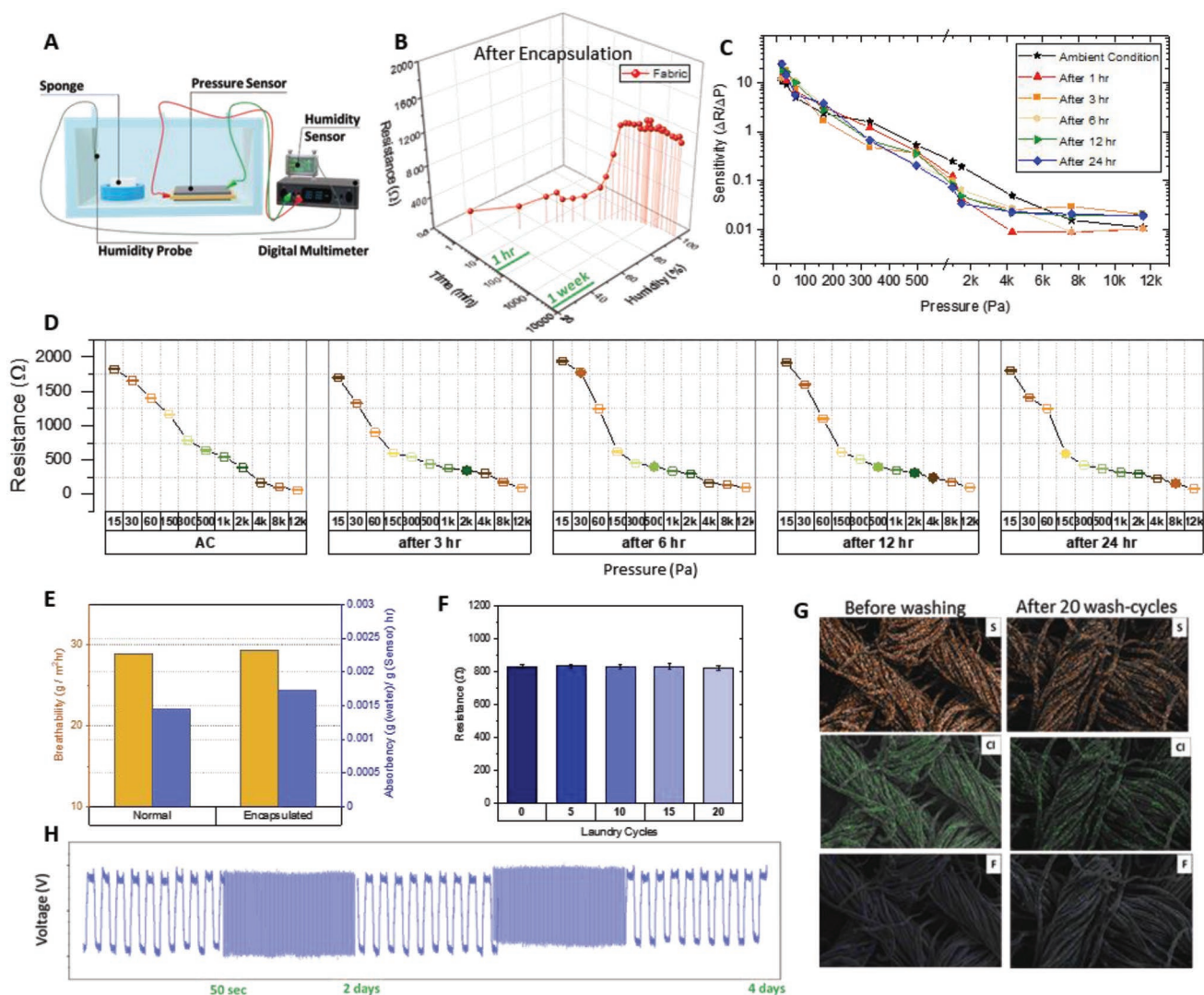
**ADVANCED
SCIENCE NEWS**

www.advancedsciencenews.com

**ADVANCED
MATERIALS
TECHNOLOGIES**

www.advmattechnol.de

Figure 3. Effect of encapsulation on breathability and performance of the sensor as exposed to humidity, laundry, and cycling: A) experimental setup for long-term evaluation of the sensor performance over the change in humidity. B) Change in the sensor resistance upon the increase in humidity over a 7-day measurement. C) Change in the sensitivity of the sensor while being exposed to ≈100% relative humidity (RH) for 1, 3, 6, 12, and 24 h. D) Boxplot of the sensor signal variation while being exposed to ≈100% RH for 3, 6, 12, 24 h. E) Bar plot illustration of the sensors breathability and absorbency before and after being encapsulated. F) Bar plot illustration of the change in sensor resistance after laundering the sensor with detergent. G) SEM image and elemental map obtained using EDX of the sensor active layer before and after 20 laundry cycles for Sulfur (S), Chlorine (Cl), and Fluorine (F) from top to bottom, respectively, H) working stability test of the sensor with more than 70 000 bending cycles (4 days) shows 99.21% performance retention in ambient condition.

does not allow water molecules to hydrate PEDOT-Cl coating and thus protects the sensor from resistance drop.

Then we re-evaluate the sensitivity and range of variation of the sensor as exposed to ≈100% RH before and after being encapsulated. We reperformed the experiment explained before with applying static pressure through a variety of weights. Figures S7 and S8 (Supporting Information) reveals the change in sensitivity and the resistance variations, respectively, for the sensor without the protective layer. A decline in sensitivity magnitude can be observed after 6 h of exposure to ≈100% RH. In contrast, in the presence of the protective layer, the sensitivity and range of variation had less than no change even after 24 h of exposure to 100% RH (Figure 3C,D).

2.6. Breathability, Laundry, and Working Stability of the Sensor

High breathability is considered another important feature of comfortability for daily adaptability of a wearable sensor. In order to measure the breathability of the sensor and investigate the effect of hydrophobic layer on this important feature, we tightly placed the sensor over a container filled with activated drierite, and let them both sit in the humidity chamber for 24 h. We measured the amount of water vapor absorbed by the sensor as a measure of absorbency of the sensor, and the amount of water vapor passed through the sensor and absorbed by the drierite as a measure of its breathability. The absorbency

data were normalized by the weight of the sensors. As seen in Figure 3E, not only the encapsulation had less than no negative effect on the breathability of the sensor, but also the encapsulated sensors showed an slight increase in absorbency and breathability, respectively. Although, the increase in absorbency in the sensor with hydrophobic layers sound counter intuitive, it must be noted that the water absorbed by the sensor was penetrated in the free volumes between the fibers and did not wet the fibers. This free volume had slightly expanded as the hydrophobicity of the fibers make them repel each other when exposed to water molecules, leading to higher amount of absorbency and breathability.

When it comes to wearable sensors that are supposed to be embedded in daily garments, laundry stability becomes very challenging. Applying the encapsulation layer on the sensor successfully addressed this challenge. As revealed in Figure 3F, after each five cycles of laundry, the dynamic test was performed on the sensor, as explained before in Figure 2F, and the output signal does not drop even after 20 cycles of laundry. In the washing process, the water only holds to the outer layer of the sensor and barely penetrates the inner layers, and even if it does, it cannot affect the conductive PEDOT-Cl coating. The EDX elemental map of the sensor confirmed the persistence of Sulfur (S), Chlorine (Cl), and Fluorine (F) atoms within the active layer even after enduring 20 laundering cycles with laundry detergent (Figure 3G).

Working stability in the ambient condition is also quite an issue in wearable technology specially piezoresistive pressure sensors. The sensor must tolerate all the abrasion and mechanical deformation resulted from body/joint movements in daily life. To simulate this condition, we took advantage of an artificial arm and imposed the sensor under the application of bending cycling continuously for 4 days. As shown in **Figure 4**E, the sensor revealed 99.21% performance retention even after more than 70 000 consistent bending cycles, which is exceedingly higher than the reported counterparts.[37]

2.7. Proof of Concept

One of the great advantages of our designed fabric-based pressure sensor as compared to other mount-on-skin or tight-fitting pressure sensors is that this sensor can be embedded in loose clothing. The key idea of this design is that there are some locations on the body that are both critical for acquiring physiological signals and can be pressed against another surface such as body torso, bed, or arm. By leveraging those key locations and to validate the performance of our pressure sensor, we gently placed the pressure sensor on a participant's body and extracted a plethora of various physiological signals and body motions. It is worth mentioning that the cytotoxicity of both PEDOT-Cl and TCPFS coatings was assessed in vitro and resulted in zero reactivity which means that they are safely biocompatible for user studies and further biomedical applications (Table S1, Supporting Information). For respiration signal (**Figure 5**A), we asked the participant to lie face down on a bed, while placing the sensor between the chest and the bed. It is also possible to capture the same respiration signal by having the sensor on the participant' back, while the participant is lying face-up over it.

The heartbeats were recorded by placing the sensor on the side, between the arm and torso using a loose-fitting shirt (Figure 5D) and at the same time the participant's electrocardiography (ECG) signal was also acquired as the ground truth. External jugular vein pulses were captured by placing the sensor on the neck pressed by the collar of the participant's shirt (Figure 5B), while its ECG ground truth was simultaneously being recorded. A reliable signal output was captured when the participant placed the sensor on the inside of the elbow allowing for motion detection at joints (Figure 5C). To verify the stability of our sensor performance against sweat, we simulated the human body perspiration by spraying 100 mM saline over the sensor every 30 min, while the participant was wearing it in the elbow. We collected the elbow bending signal with a constant rate and angle after 1 and 3 h. As seen in Figure 5E, no degradation in the sensor performance was observed after 3 h of exposure to sweat. Finally, by asking the participant to walk while the sensor was embedded as an insole in their footwear, we obtained a persistent signal output (Figure 5F) which can be leveraged for footwear evaluation studies. Each and every one of these signals suggests a promising platform to perform deeper kinesiological and physiological studies and their corresponding niche applications.
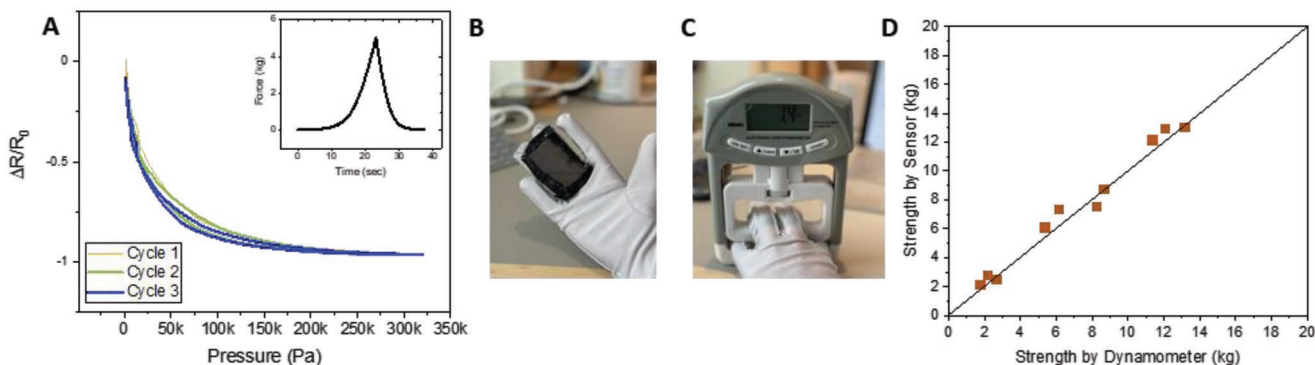

Figure 4. Performing Grip Strength Measurement comparable to the commercial dynamometers: A) Change in $\Delta R/R_0$ over loading and unloading a compression stress on the sensor for three consecutive cycles. B) photograph of the sensor embedded in a fabric glove for grip strength measurement. C) Photograph of the experimental setup for comparing the strength read by the sensor versus the one read by the dynamometer. D) Relationship between the grip strength acquired by the sensor and by the dynamometer. The correlation coefficient of the results by the sensor and the dynamometer is 0.936.
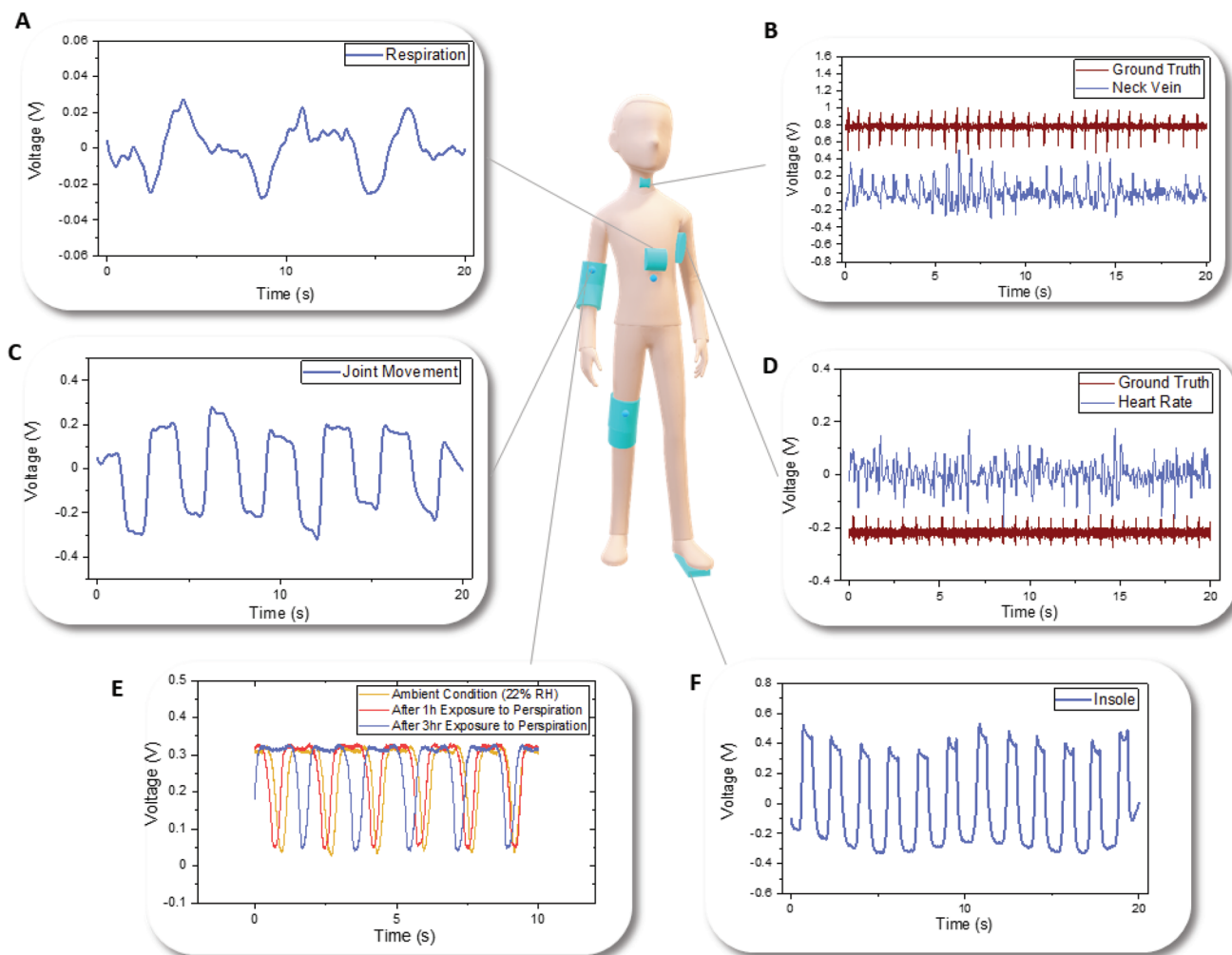
Figure 5. Extracting a variety of physiological signals and body motions by placing the sensor on different body locations. A) respiration from the sensor placed on chest while lying face down on a bed. B) External jugular vein pulses from the sensor placed on the neck pressed by the collar. C) Joint motion from the sensor placed at the knee or elbow. D) Heartbeats from the sensor placed between the arm and torso while sitting on a chair. E) Joint motion from the sensor placed at the elbow after exposure to perspiration for 1 and 3 h. F) Steps from the sensor used as an insole in footwear.

2.8. Grip Strength Measurement

While grip strength, or simply muscular strength, is an important health indicator specially for rehabilitation patients, athletes, and babies, still there is no wearable sensor being able to be comfortably and accurately used for personalized grip strength detection, not only for adults but also for the entire target population. Here we embedded our sensor into a glove and successfully performed grip measurements.

First, we calibrated the sensor by measuring the change in its resistance while loading and unloading a compression stress on the sensor for three consecutive cycles. The compression force was applied to the sensor up to 7 kg with the rate of 0.1 mm s^{-1} and then returned to the first position with the same rate. As shown in Figure 4A, the sensor shows a slight hysteresis effect representative of piezoresistive sensors. Then, we asked a participant to wear the embedded glove and apply a pressure to the commercial dynamometer with their two fingers covered by the sensor, while we were reading the change in the resistance of

the sensor (Figure 4B and C). By normalizing the data based on the contact surface area, as revealed in Figure 4D, the correlation coefficient of the grip strengths acquired by the sensor and the dynamometer is 0.936. This result is quite appealing for a fabric-based wearable sensor enabling long-term monitoring of grip strength in an effective, robust, and versatile manner.

3. Conclusion

In summary, oCVD PEDOT-Cl coated textiles have been put forward for fabrication of a high-performance electromechanical pressure sensor. This one-step technique allowed us to tune the conductivity and subsequently sensitivity of the sensor accordingly. We observed that the sensor enjoyed a multiscale working mechanism, in which we had the putative decrease in the thickness and therefore reduction in the air trapped in the free volume of the active layer in milli-centimeter scale, the percolation pathways in micro-millimeter scale, and piezoionic

**ADVANCED
SCIENCE NEWS**

www.advancedsciencenews.com

**ADVANCED
MATERIALS
TECHNOLOGIES**

www.advmattechnol.de

effect in nanometer scale. This multiscale sensitivity was the key to its broad RoD along with its ability to simultaneously detect subtle dynamic and static pressure in the presence of a base pressure. The vapor deposited encapsulation layer greatly improved the stability of the sensor against humidity and laundry cycling. The sensitivity of the sensor displayed no significant change even after exposure to 100% RH and more than 70 000 bending cycles. Physiological signals and human activities can be simply captured through this all-fabric sensor which can be embedded in loose-fitting daily garments with no degradation upon the exposure to perspiration. To the best of our knowledge, this is the first fabric-based wearable sensor used for grip strength measurement with up to 93.6% accuracy, while covering a wider range of detection as compared to commercial dynamometers enabling its long-term personalized application for sensitive populations such as babies and rehabilitation patients. The combination of these properties along with the low-cost and robust fabrication process of this sensor exceeds that of the ones reported so far which will enable a host of cutting-edge biomedical and human–computer interaction applications.

4. Experimental Section

Materials: 3,4-ethylenedioxythiophene (EDOT) (>95.0%) was purchased from TCI America. Iron(III) Chloride (97%) ($FeCl_3$), trichloro (1H,1H,2H,2H-perfluorooctyl)silane (TCPFS) were purchased from Sigma-Aldrich. Methanol and Hydrochloric acid (36.5–38.0% w/w) were purchased from Fisher Scientific. All chemicals were used without further purification. Silver plated (76%) nylon (24%) was purchased from Less EMF Inc. Cotton voile fabric and regular cotton fabric were purchased from Joanne Fabrics and organic cotton balls were purchased from SkyOrganics. All the fabrics used in this study were prewashed and then sonicated with Isopropanol and allowed to dry in the ambient condition.

Vapor Deposition of PEDOT-Cl on Active Layer: Vapor phase deposition of PEDOT-Cl was conducted in a home-built hot wall reactor depicted in Figure 1. Briefly, EDOT monomers were evaporated at 95 °C and delivered into the chamber via inlet controlled by a need valve typically opened a quarter turn with a constant flow rate of 10 sccm. Inside the chamber, $FeCl_3$ was sublimed by heating to >250 °C in a Luxel RADAK II furnace. The EDOT reacted with $FeCl_3$ in the vapor phase at almost constant pressure of 750 mTorr and the polymer film deposited on the substrate stage (cotton voile fabric or cotton balls) heated to 150 °C over the course of deposition. A quartz crystal microbalance (QCM) located inside the reactor was used for real-time monitoring the film growth rate. Since the QCM had a different position relative to the stage, a tooling factor of 0.5 was calculated. Film growth rate was almost constant at 5 nm s^{-1}. The sample were immediately rinsed with 0.5 M HCl followed by methanol to remove the residual monomer and oxidant and then allowed to dry in the ambient condition.

Encapsulation: A 10 min deposition of TCPFS was conducted on the PEDOT-Cl coated cotton voile, PEDOT-Cl coated Cotton ball, regular cotton (frames), and silver-plated nylon. This deposition was conducted in another custom-built chamber at a constant pressure of 1 Torr. The TCPFS was evaporated at 80 °C outside the chamber and was introduced into the chamber through an inlet with a constant flow controlled by a needle valve.

Fabrication of the Pressure Sensor: The pressure sensor was a 7×15 cm² patch composed of two 5×13 cm² sheets of silver-plated nylon, the two of which were sewn onto two 2×15 cm² sheets of regular cotton working as the frame to prevent the occurrence of shorting in the sensor.

Then the PEDOT-Cl coated textiles (either cotton voile or cotton ball) were placed between the electrodes and the final pressure sensor was ready by sewing together two ends of the frames around the perimeter. In the case of using PEDOT-Cl coated cotton ball as the active layer, the coated cotton balls were thoroughly fluffed up by hand to get an almost uniform dispersion of coated yarns in the whole 3D textile.

Chemical and Electric Characterization: Field-emission scanning electron microscopy (SEM) and energy-dispersive X-ray spectroscopy (EDX) were performed using a Magellan 400 microscope. All the electrical resistance directly reported in this study were measured using a FLUKE 8846A digit precision multimeter.

Low-Temperature Conductivity Measurement: The low-temperature measurement was performed in a custom-built chamber (reported in[38]). Briefly, using a PID controller (J-KEM Gemini), an aquarium pump bubbled air through the liquid nitrogen and then the introduced it into the chamber. The sensor was held at the target temperature for at least 10 min before each measurement. Then, the IR drop in galvanostatic charge–discharge test was conducted using a WaveNow Potentiostat (Pine Instrument). A charging current of 100 µA was used.

Contact angle measurement was performed using a Bolin Scientific Attention Optical Tensiometer, and the data were analyzed using OneAttention software. The video was captured at 14 FPS. The measurement was performed 5 times, each time using a 10 µL droplet of ultrapure water (acquired using Thermo Scientific Micropure UV/UF).

Wash Stability: The wash stability test was conducted by stirring the sensor at 300 rpm in the solution of water and laundry detergent (100:1 v/v) at 30 °C for 15 min. Then the sensor was rinsed with water for 5 min and allowed to dry at ambient condition.

Cytotoxicity Test: The cytotoxicity of the PEDOT-Cl coated active layer and the encapsulation layer were carried out by a third-party lab, Nelson Laboratories (Salt Lake City, UT), in accordance with criteria established by US Pharmacopeia and National Formulary (USP 87) and ANSI/AAMI/ISO 10993-5 standards. The cytotoxicity was assessed in vitro on a culture of mouse fibroblast cells (standard L-929) (ATCC CCL-1). The results are summarized in Table S1 (Supporting Information), and the report from Nelson lab will be available upon request.

Compression Test: The compression loading–unloading cycles were performed using a Texture Analyzer from "Stable Micro Systems". The probe was a cylinder probe with a diameter of 25 mm. The travelling arm was set at 0.5 mm of the sensor and was fitted with a 5 kg load cell. The loading and unloading cycles of compression were performed at the rate of 0.1 mm s^{-1}.

Supporting Information

Supporting Information is available from the Wiley Online Library or from the author.

Acknowledgements

Conflict of Interest

The authors declare no conflict of interest.

Data Availability Statement

The data that support the findings of this study are available from the corresponding author upon reasonable request.

[1] H. Liu, S. Zhang, Z. Li, T. J. Lu, H. Lin, Y. Zhu, S. Ahadian, S. Emaminejad, M. R. Dokmeci, F. Xu, A. Khademhosseini, *Matter* **2021**, *4*, 2886.

[2] K. Meng, S. Zhao, Y. Zhou, X. Tan, J. Yang, J. Chen, Y. Wu, S. Zhang, Q. He, X. Wang, Z. Zhou, W. Fan, *Matter* **2020**, *2*, 896.

[3] S. Majumder, T. Mondal, M. Deen, *Sensors* **2017**, *17*, 130.

[4] T. L. Andrew, *Matter* **2020**, *2*, 794.

[5] S. Z. Homayounfar, T. L. Andrew, *SLAS Technol.* **2020**, *25*, 9.

[6] G. Schwartz, B. C. K. Tee, J. Mei, A. L. Appleton, D. H. Kim, H. Wang, Z. Bao, *Nat. Commun.* **2013**, *4*, 1858.

[7] A. Kiaghadi, S. Z. Homayounfar, J. Gummeson, T. Andrew, D. Ganesan, *Proc. ACM Interact. Mob. Wearable Ubiquitous Technol.* **2019**, *3*, 89.

[8] H. Zhang, X. Ding, X. Zhang, F. Xu, *Npj Flex Electron.* **2022**, *6*, 28.

[9] B. Dresp-Langley, *Advances in Biosensors: Reviews*, Vol. *3*, (Eds.: S. Y. Yurish), International Frequency Sensor Association (IFSA), **2020**, pp. 107–122.

[10] D. P. Leong, K. K. Teo, S. Rangarajan, P. Lopez-Jaramillo, A. Avezum, A. Orlandini, P. Seron, S. H. Ahmed, A. Rosengren, R. Kelishadi, O. Rahman, S. Swaminathan, R. Iqbal, R. Gupta, S. A. Lear, A. Oguz, K. Yusoff, K. Zatonska, J. Chifamba, E. Igumbor, V. Mohan, R. M. Anjana, H. Gu, W. Li, S. Yusuf, *Lancet* **2015**, *386*, 266.

[11] A. García-Hermoso, I. Cavero-Redondo, R. Ramírez-Vélez, J. R. Ruiz, F. B. Ortega, D. C. Lee, V. Martínez-Vizcaíno, *Arch. Phys. Med. Rehabil.* **2018**, *99*, 2100.

[12] F. Lunardini Politecnico di Milano, I. N. Alberto Borghese, S. Srl, I. Giuseppina Bernardelli, M. Cesari, F. Lunardini, *Health Informatics J.* **2020**, *26*, 1952.

[13] S. R. A. Ruth, V. R. Feig, H. Tran, Z. Bao, *Adv. Funct. Mater.* **2020**, *30*, 2003491.

[14] H. Ceren Ates, P. Q. Nguyen, L. Gonzalez-Macia, E. Morales-Narváez, F. Güder, J. J. Collins, C. Dincer, *Nat. Rev. Mater.* **2022**, *7*, 887.

[15] X. Wei, H. Li, W. Yue, S. Gao, Z. Chen, Y. Li, G. Shen, *Matter* **2022**, *5*, 1481.

[16] S. Pyo, J. Lee, K. Bae, S. Sim, J. Kim, *Adv. Mater.* **2021**, *33*, 2005902.

[17] C. L. Choong, M. B. Shim, B. S. Lee, S. Jeon, D. S. Ko, T. H. Kang, J. Bae, S. H. Lee, K. E. Byun, J. Im, Y. J. Jeong, C. E. Park, J. J. Park, U. I. Chung, *Adv. Mater.* **2014**, *26*, 3451.

[18] Y. Wang, M. Zhu, X. Wei, J. Yu, Z. Li, B. Ding, *Chem. Eng. J.* **2021**, *425*, 130599.

[19] H. Zhang, C. Li, W. Ning, H. Chen, *Mater. Lett.* **2022**, *307*, 130977.

[20] L. Pan, A. Chortos, G. Yu, Y. Wang, S. Isaacson, R. Allen, Y. Shi, R. Dauskardt, Z. Bao, *Nat. Commun.* **2014**, *5*, 3002.

[21] B. Ju, I. Kim, B. M. Li, C. G. Knowles, A. Mills, L. Grace, J. S. Jur, *Adv. Healthcare Mater.* **2021**, *10*, 2100893.

[22] S. Honda, Q. Zhu, S. Satoh, T. Arie, S. Akita, K. Takei, *Adv. Funct. Mater.* **2019**, *29*, 1807957.

[23] J. Zhao, Y. Fu, Y. Xiao, Y. Dong, X. Wang, L. Lin, *Adv. Mater. Technol.* **2020**, *5*, 1900781.

[24] S. Wu, M. Zou, X. Shi, Y. Yuan, W. Bai, M. Ding, A. Cao, *Adv. Mater. Technol.* **2019**, *4*, 1900470.

[25] X. Ding, W. Zhong, H. Jiang, M. Li, Y. Chen, Y. Lu, J. Ma, A. Yadav, L. Yang, D. Wang, *ACS Appl. Mater. Interfaces* **2020**, *12*, 35638.

[26] S. J. Park, J. Kim, M. Chu, M. Khine, *Adv. Mater. Technol.* **2018**, *3*, 1700158.

[27] H. Zhao, Y. Zhou, S. Cao, Y. Wang, J. Zhang, S. Feng, J. Wang, D. Li, D. Kong, *ACS Mater. Lett.* **2021**, *3*, 912.

[28] W. Zhong, C. Liu, Q. Liu, L. Piao, H. Jiang, W. Wang, K. Liu, M. Li, G. Sun, D. Wang, *ACS Appl. Mater. Interfaces* **2018**, *10*, 42706.

[29] W. Zhong, H. Jiang, K. Jia, X. Ding, A. Yadav, Y. Ke, M. Li, Y. Chen, D. Wang, *ACS Appl. Mater. Interfaces* **2020**, *12*, 37764.

[30] X. Li, X. Li, Ting liu, Y. Lu, C. Shang, X. Ding, J. Zhang, Y. Feng, F. J. Xu, *ACS Appl. Mater. Interfaces* **2021**, *13*, 46848.

[31] J. Zhang, L. Wan, Y. Gao, X. Fang, T. Lu, L. Pan, F. Xuan, *Adv. Electron. Mater.* **2019**, *5*, 1900285.

[32] S. Z. Homayounfar, A. Kiaghadi, D. Ganesan, T. L. Andrew, *J. Electrochem. Soc.* **2021**, *168*, 017515.

[33] S. Z. Homayounfar, S. Rostaminia, A. Kiaghadi, X. Chen, E. T. Alexander, D. Ganesan, T. L. Andrew, *Matter* **2020**, *3*, 1275.

[34] S. Chen, W. H. Li, W. Jiang, J. Yang, J. Zhu, L. Wang, H. Ou, Z. Zhuang, M. Chen, X. Sun, D. Wang, Y. Li, *Angew. Chem., – Int. Ed.* **2022**, *61*, 202114450.

[35] X. B. Chen, J. P. Issi, M. Cassart, J. Devaus, D. Billaud, *Polymer* **1994**, *35*, 5256.

[36] L. K. Allison, S. Rostaminia, A. Kiaghadi, D. Ganesan, T. L. Andrew, *ACS Omega* **2021**, *6*, 31869.

[37] C. Lu, X. Liao, D. Fang, X. Chen, *Nano Lett.* **2021**, *21*, 5369.

[38] W. Viola, T. L. Andrew, *J. Phys. Chem. C* **2021**, *125*, 246.